Universiteit
Antwerpen

This item is the archived peer-reviewed author-version of:

Mechanisms for plasma cryogenic etching of porous materials

Reference:
Zhang Quan-Zhi, Tinck Stefan, de Marneffe Jean-François, Zhang Liping, Bogaerts Annemie.- Mechanisms for plasma cryogenic etching of porous materials
Applied physics letters / American Institute of Physics - ISSN 1077-3118 - 111:17(2017), 173104
Full text (Publisher's DOI): http://dx.doi.org/doi:10.1063/1.4999439

uantwerpen.be
Institutional repository IRUA

Mechanisms for plasma cryogenic etching of porous materials

Quan-Zhi Zhang,[1, a)] Stefan Tinck,[1] Jean-François de Marneffe,[2] Liping Zhang,[2] and Annemie Bogaerts[1]

[1]*Research Group PLASMANT, University of Antwerp, Universiteitsplein 1, B-2610 Antwerp-Wilrijk, Belgium*

[2]*IMEC, Leuven 3001, Belgium*

Porous materials are commonly used in microelectronics, as they can meet the demand for continuously shrinking electronic feature dimensions. However, they are facing severe challenges in plasma etching, due to plasma induced damage. In this paper, we present both the plasma characteristics and surface processing during the etching of porous materials. We explain how the damage occurs in the porous material during plasma etching for a wide range of chuck temperatures, and the responsible mechanism for plasma damage-free etching at cryogenic temperature, by a combination of experiments and numerical modeling.

As the electronic feature dimensions in the semiconductor industry are continuously shrinking, porous materials are increasingly being used as inter-metal insulators to address the critical need for low dielectric constant (low-k).[1-5] However, a lower dielectric constant normally requires increased pore size and interconnectivity, which will induce a high sensitivity to plasma processing, as radicals and ions can easily penetrate into the interconnected pores, causing severe damage and degrading the dielectric properties.[6-11] Especially when the feature dimensions drop to 14 nm,[12] the damage depth can be comparable with the narrow trench structures,[13-14] which will result in a significant degradation of the low-k material quality and a non-optimal isolation of adjacent metal lines. Therefore, protection of porous material becomes crucial during plasma processing**.**

Among many different protection strategies,[12, 15-19] the pore stuffing approaches are the most straightforward and efficient way.[16-19] By filling the pores with polymer material, the penetration of radicals can be impeded, allowing the protection of the porous material. Compared to traditional pore stuffing approaches with pore stuffing and de-stuffing processes, an alternative protection approach, still at the research phase, was recently proposed,[14] and it also shows high potential for limited plasma induced damage (PID) during plasma etching. By cooling the wafer to cryogenic temperature in fluorocarbon based gas (e.g., C_4F_8, C_6F_6) before plasma processing, this gas may condense in the pores as liquid, which can prevent the diffusion of radicals in the interconnected pores during the subsequent plasma etching. Finally, after etching, the wafer is brought back to room temperature, so that the condensed gas will evaporate, releasing the pores again. Although the concept of cryogenic filling is simple, the underlying mechanisms can be quite complicated, as the cryogenic temperature and filling can both affect the plasma behavior. All previous research on cryogenic pore filling is solely experimental, which is very valuable but provides limited insights. The inherent mechanisms and the interaction between the plasma and 'pore filling', remain indeed very poorly understood.

In this work, we will describe the responsible mechanisms for damage-free cryogenic etching of porous low-k material, both experimentally and numerically. Our simulations will show how the PID evolves in the inter-connected pores, how the protection happens in the pores filled with condensed material, and how the plasma behaves at cryogenic temperature when the pore is filled. The insights obtained from this work are, however, not limited to cryogenic etching, and they might apply to other stuffing protection strategies for porous materials as well.

[a)] Author to whom correspondence should be addressed. Electronic mail: Quan-Zhi.Zhang@uantwerpen.be

To experimentally examine the protection effect of porous material in condensation-based cryogenic etching, porous organosilicate low-k dielectric material, indicated as p-SiOCH, with 46% open porosity and 1.7 nm pore radius is being etched by an inductively coupled plasma (ICP) in a mixture of C_4F_8 and SF_6. The etching is conducted at different chuck temperatures, and all the samples are dipped into 0.5% diluted hydrofluoric (dHF) acid liquid for 30s after etching. Dipping in dHF is used to evaluate the degree of PID, as the bonds of terminal Si-CH_3 group in p-SiOCH can protect the low-k matrix from dHF, but the PID will remove the CH_3 groups from the pores of p-SiOCH, which makes the porous material chemically reactive with dHF.[20] Therefore, after dipping into dHF acid, cross sectional inspection will point out which part of the material is damaged by plasma species and removed by dHF.

Figure 1 shows a cross section of the obtained etching profiles, measured by scanning electron microscopy (SEM). At -50 °C, both the trench bottom and sidewalls are roughly etched (top left corner), as the F-containing radicals from the plasma penetrate into the pores and react with the internal material. Furthermore, the trench sidewalls (patterned structure) are completely removed after dipping in dHF (top right corner). This indicates that significant chemical reactions occurred throughout the sidewalls separating two trenches, i.e. the sidewall damage depth exceeds the spacing width. In contrast, the surface roughness after plasma etching is much improved, and all the trench sidewalls are preserved under the protection of condensed C_4F_8 gas at -110 °C (see bottom left and right corner of Figure 1).

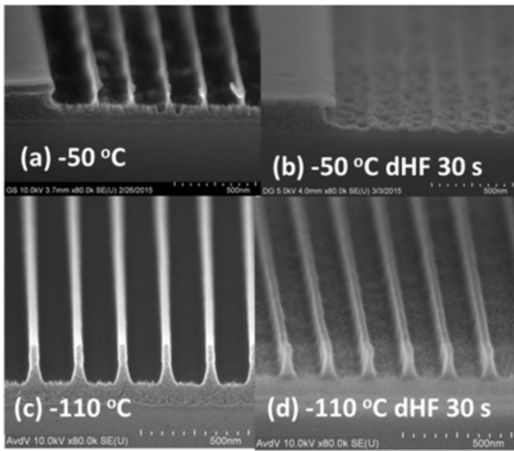

FIG. 1. Cross sectional images of narrow spacing trench profiles (30nm low-k line at 180nm pitch) by SEM after plasma etching (left) and 0.5% dHF dip (right), at -50°C (top) and -110°C (bottom)

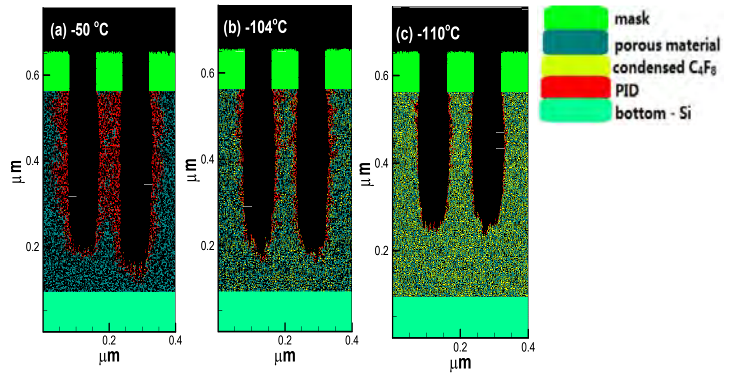

FIG. 2. Calculated trench profiles after plasma etching for 160 s, at (a) -50 °C (no pore filling), (b) -104 °C (15% filling), (c) -110 °C (50% filling) (Multimedia view (a), (b), (c))

To examine what is exactly happening inside the pores during etching, we study the etching mechanisms of two adjacent narrow trenches, made of porous SiO_2 dielectric material, by means of a 2D Monte Carlo model, which forms part of a hybrid plasma model.[21-22] More details about this model, as well as the chemistry included in the model (i.e., list of species, reactions in gas phase and at surface) can be found in the Supplementary Material.

We study the etching mechanisms for different filling degrees of the porous material. We calculate the filling percentage of the pores based on the variation of refractive index measured from experiments, as in Ref. 14. Furthermore, based on the measured dependence of the refractive index on chuck temperature in Ref. 16, we can estimate the filling percentage at different chuck temperature (see detailed explanation in the Supplementary Material).

In our model, we consider 3 different scenarios, i.e. no filling (or 100% porous) at -50 °C, 15% filling at -104 °C, (d) 50% filling at -110 °C. Although the pores are completely interconnected in three-dimensional space in case of no filling, it is not

possible to have a 100% connected porous network in a 2D model, as the pores need to be randomly located in the cross section of the material. We thus consider a somewhat larger porosity of 60% (instead of 46% in the experiments) to account for the larger interconnectivity, when comparing with the experimental data. The average pore radius is also 1.7 nm, like in the experiments. The condensed C_4F_8 uniformly fills up the pores from the edges to the centre at increasing filling degree. A calculated self-bias of -115 V develops on the RF electrode, which corresponds to the experimental self-bias of -120 V.

Figure 2 shows the calculated etch profiles at different chuck temperatures (corresponding to the different pore filling percentages mentioned above), for a fixed etch time of 160 s. The red color, most clearly observed in Figure 2(a), indicates the permeation of plasma species and their reactions with the pores, leading to PID. The interconnected porous network acts as channels for the penetration of F-containing radicals, causing severe damage to the material stucture. This can be obsered more clearly from the etching movies in the supporting information of this paper. Especially the middle trench sidewall becomes damaged from two sides at the same time. In the end, it will become severely damaged, and the main part of the middle trench will be removed by dHF, which corresponds to the experimental results in Figure 1 (a) and (b). Indeed, in practice, more channels will be created as the damage develops, finally crossing each other, so that the radicals can diffuse deeper and deeper.

When lowering the temperature to -104 °C (corresponding to 15% pore filling), the two etched trenches become absolutely independent and the penetration of radicals in the sidewalls is significantly impeded; see Figure 2(b). At -110 °C (50% pore filling), there are almost no penetration channels anymore (see Figure 2(c)), and the porous material starts to become well protected, as most pores will be separated from each other, and the penetration channels cannot be developed. The etching profile corresponds to the experimental results in Figure 1 (c) and (d). When further lowering the temperature to -115 °C and -120 °C, the porous material can be almost perfectly protected (see Supplementary Material for etch profiles at -95 °C, -115 °C and -120 °C). Hence, upon lowering the chuck temperature (and thus rising the pore filling degree), the material can gradually be protected, but on the other hand, the etch rate also decreases, which can be deduced from the decreased etch depths with lowering chuck temperature for the same etch time in Figure 2.

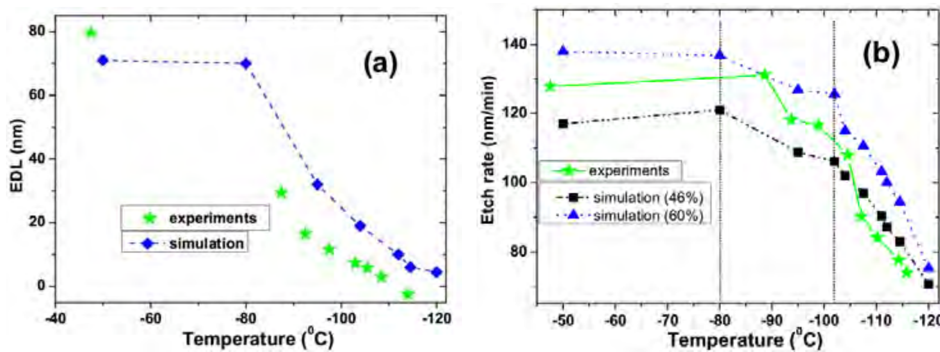

FIG. 3. (a) Equivalent damage layer (EDL) obtained from the experiments using Fourier Transform Infrared Spectroscopy, and from the simulations by averaging the damage depth along the trench sidewall; (b) experimental etch rate at 46% porosity (derived from Ref. 14), and obtained from the simulations at 46% and 60% porosity.

To quantitatively evaluate the extent of damage at different chuck temperatures (and thus pore filling degrees), we plot the average damage depth, or the so-called equivalent damage layer (EDL), as a function of chuck temperature in Figure 3(a), as obtained from the experiments and simulations. The same trend can be observed for both the experiments and simulations. The EDL decreases monotonously upon lower chuck temperature below -80 °C (i.e., the temperature at which C_4F_8 starts condensing[14]) because C_4F_8 condenses inside the pores, which significantly reduces the number of penetration channels

between the pores. The EDL values from both experiments and simulation become extremely small when the temperature approaches -110 °C.

The condensed C_4F_8 is mainly removed by ion bombardment, and that explains why the etching takes place in the vertical direction and not in the horizontal direction, as the ions are accelerated by the electric field, arriving at the wafer in the perpendicular direction, and thus they mainly bombard the trench bottom and not the sidewalls. In figure 3(b) the etch rate is plotted as a function of chuck temperature, as obtained from the experiments at 46% porosity, as well as from the simulations, both at 46% and 60% porosity. A good qualitative agreement is achieved between the experiments and simulation results.

The variation in etch rate upon decreasing chuck temperature can be generally divided into 3 segments, as indicated in figure 3(b): from -50 °C to -80 °C, from -80 °C to -102 °C, and from -102 °C to -120 °C. Between -50 °C and -80 °C, the etch rate is nearly constant, as there is virtually no filling inside the pores. The slight change in etch rate is because of the variation in fluxes of the plasma species arriving at the wafer at different chuck temperatures. Between -80 °C and -102 °C, the pores are gradually filled to a certain degree. Since the filling should first be removed by ion sputtering before etching can take place, the etch rate is thus reduced. However, the filling degree is still quite small (< 15%) within this temperature range, so the reduced connectivity between the pores can still be quite easily repaired, and the total etch rate decreases only moderately. Between -102 °C and -120 °C, the degree of filling increases from 15% to 100%, and the more significant drop in etch rate upon lowering the chuck temperature is largely attributed to the more difficult removal of the filling inside the pores. Meanwhile, the variation of plasma characteristics (see below) also affects the etch rate to a certain degree.

To better understand the responsible mechanisms and plasma behavior in cryogenic etching, we further examine the distributions of plasma species (F and C_2F_4) and ion energy bombarding the wafer at -50 °C and -120 °C in figure 4.

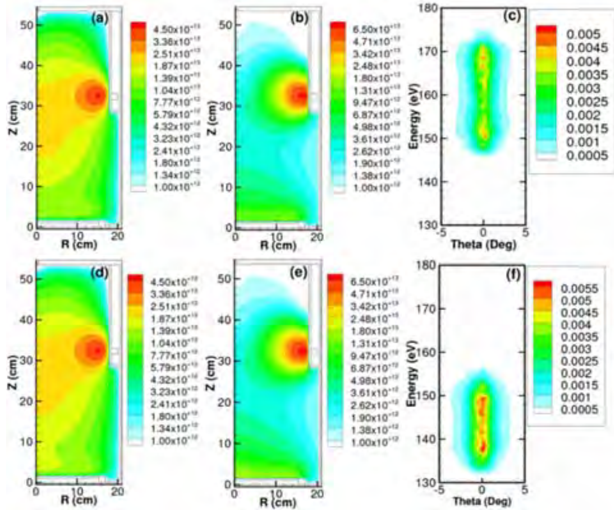

FIG. 4. Calculated (a,d) F atom density (in cm^{-3}), (b,e) C_2F_4 molecule density (in cm^{-3}) and (c,f) normalized ion energy and angular distributions, at -50 °C (a,b,c) and -120 °C (d,e,f) .

Both F and C_2F_4 reach a maximum density near the coil at both temperature of -50 °C and -120 °C. This is because of the strongest electromagnetic field at this position, and consequently most ionization and dissociation reactions take place here. However, the gas number density becomes higher at lower gas temperature (following the ideal gas law), which can induce a higher collision frequency, and therefore, a somewhat higher F and C_2F_4 density appears above the bottom electrode at -120 °C (see yellow color). Since the C_2F_4 molecules have a much higher mass than the F atoms, they will not be so much affected by diffusion, and therefore, the increase of the C_2F_4 concentration above the bottom electrode is a bit more

pronounced. This induces a 17% increase for the F flux, vs. 32% increase for the C_2F_4 flux to the wafer at -120 °C. Although F is the main reactive etching species, C_2F_4 contributes to the passivation layer on the material and the etching only happens after removing this passivation layer by reactions with F atoms and ion sputtering.[22] Therefore, the relatively higher increase in C_2F_4 flux with lower temperature may also reduce the etch rate. Furthermore, the higher concentration of all neutrals enhances the collision frequency between the species above the wafer at low temperature, which induces a smaller self-bias. Indeed, the self-bias is always lower in a collisional plasma than in a collisionless plasma.[23] Consequently, there is a drop of almost 20 eV in the ion energy. This also contributes a bit to the lower etch rate.

In conclusion, we have explored the evolution of plasma damage inside porous material as a function of chuck temperature and the responsible protection mechanism by cryogenic etching. The results of the numerical model are in very good agreement with the experimental data, so the model allows to provide insight in the protection strategy of porous material processing. The interconnected porous network acts as penetration channels for the radicals, which causes deep damage into the material stucture, and it can even destroy the dielectric spacing, leading to structure loss. When lowering the chuck temperature, the C_4F_8 gas used for pore stuffing gradually condenses inside the porous material and fills the pores. This pore filling can mitigate the PID at the sidewalls, and also reduce the connectivity between the pores, i.e., the penetration channels of the radicals, which decreases the damage depth into the material. When the pore filling degree reaches 50%, the porous material starts to become well protected. However, since the filling first needs to be removed by ion sputtering before etching can proceed, the etch rate is also significantly reduced upon lowering the chuck temperature. Therefore, a chuck temperature around -104 °C might be more beneficial, as it yields limited damage (in spite of the moderate filling degree of 15%), while still allowing significant etching. Meanwhile, the distributions of plasma species, and consequently the neutral fluxes and ion energy are affected by the cryogenic temperature, which also lowers the etch rate. These insights in the plasma behavior and the etch evolution help us to understand the fundamental mechanisms in cryogenic etching.

See the Supplementary Material for the more experiment and model details.

We acknowledge the support from Marie Skłodowska-Curie actions (Grant Agreement-702604). This work was carried out in part using the Turing HPC infrastructure at the CalcUA core facility of Universiteit Antwerpen, a division of the Flemish Supercomputer Center VSC, funded by the Hercules Foundation, the Flemish Government (department EWI) and the University of Antwerp. L. Zhang and J.-F. de Marneffe acknowledge Dr M. Cooke and A. Goodyear from Oxford Instruments Plasma Technology for processing the samples at their Yatton facility in United Kingdom.

[1]J. L. Hedrick, R. D. Miller, C. J. Hawker, K. R. Carter, W. Volksen, D. Y. Yoon, and M. Trollsås, Adv. Mater. **10**, 1049 (1998).
[2]R. D. Miller, Sci. **286**, 421 (1999).
[3]S. J. Martin, J. P. Godschalx, M. E. Mills, E. O. Shaffer, and P. H. Townsend, Adv. Mater. **12**, 1769 (2000).
[4]M. Baklanov, M. Green, K. Maex, Dielectric Films for Advanced Microelectronics, Wiley, New York, USA 2007**.**
[5]W. Volksen , R. D. Miller , G. Dubois , Chem. Rev. **110**, 56 (2010).
[6]Y. Furukawa, M. Patz, T. Kokubo and J. H. M. Snijders, Microelectron. Eng. **70**, 267 (2003).
[7]S. L. Xu, C. Qin, L. Diao, D. Gilbert, L. Hou, and A. Wiesnoski, J. Vac. Sci. Technol. B **25**, 156 (2007).
[8]A. Franquet, M. Claes, T. Conar, E. Kesters, G. Vereecke and W. Vandervorst, Appl. Surf. Sci. **255**, 1408 (2008).
[9]Y. Iba, T. Kirimura, M. Sasaki, Y. Kobayashi, Y. Nakata, and M. Nakaishi, Jpn. J. Appl. Phys. **47**, 6923 (2008).
[10]K. Takeda, Y. Miyawaki, S. Takashima, M. Fukasawa, K. Oshima, K. Nagahata, T. Tatsumi, and M. Hori, J. Appl. Phys. **109**, 033303 (2011).
[11]M. Darnon and T. Chevolleau, J. Vac. Sci. Technol. B **31**, 061206-1 (2013).
[12]N. Inoue, presented at IEEE Int. Electr. Dev. Meet., Washington, USA, December 2013.
[13]Q. T. Le, M. R. Baklanov, E. Kesters, A. Azioune, H. Struyf, W. Boullart, J.-J. Pireaus, and S. Vanhaelemeersch, Electrochem. Sol. St. Lett. **8**, F21 (2005).
[14]L.P. Zhang, J-F. Marneffe, F. Leroy, P. Lefaucheux, T. Tillocher, R. Dussart, K. Maekawa, K. Yatsuda, C. Dussarrat, A. Goodyear, M. Cooke, S. D. Gendt and M. R. Baklanov, J. Phys. D: Appl. Phys. **49**, 175203 (2016).
[15]O. V. Braginsky, A. S. Kovalev, D. V. Lopaev, E. M. Malykhin, Y. A. Mankelevich, T. V. Rakhimova, A. T. Rakhimov, A. N. Vasilieva, S. M. Zyryanov, and M. R. Baklanov, J. Appl. Phys. **108**, 073303 (2010).
[16]T. Frot, W. Volksen, S. Purushothaman, S. Bruce and G. Dubois, Adv. Mater. **23**, 2828 (2011)
[17]T. Frot, W. Volksen , S. Purushothaman, R. S. Bruce, T. Magbitang, D. C. Miller, V. R. Deline and G. Dubois, Adv. Funct. Mater. **22**, 3043 (2012).
[18]M. Heyne, L. Zhang, J. Liu, I. Ahmad, D. Toma, J-F. Marneffe, S. Gendt and M. R. Baklanov, J. Vac. Sci.Technol. B **32**, 062202 (2014).
[19]K. Lionti, W. Volksen, T. Magbitang, M. Darnon, and G. Dubois, ECS J. Solid State Sci. Technol. **4**, N3071-N3083 (2015)
[20]M. R. Baklanov, J. F. Marneffe, D. Shamiryan, A. M. Urbanowicz, H. L. Shi, T. V. Rakhimova, H. Huang, P. S. Ho., J. Appl. Phys. **113**, 041101 (2013).
[21]M. Kushner, J. Phys. D: Appl. Phys. **42**, 194013 (2009).
[22]A. Sankaran, M. Kushner, J. Vac. Sci. Technol. A **22**, 1242 (2004).
[23]Q. Z. Zhang, W. Jiang, L.J. Hou, and Y. N. Wang, J. Appl. Phys. 2011, 109, 013308.